Precambrian Research 266 (2015) 212–226

Contents lists available at ScienceDirect

Precambrian Research

journal homepage: www.elsevier.com/locate/precamres

Early deformation in the Eastern Goldfields, Yilgarn Craton, Western Australia: A record of early thrusting?

Louis Cohalan [a], Roberto F. Weinberg [a,*], Rick J. Squire [a], Charlotte M. Allen [b]

[a] School of Earth, Atmosphere & Environment, Monash University, Clayton, VIC 3800, Australia
[b] Institute for Future Environments, Queensland University of Technology, Gardens Point Campus, 2 George Street, Brisbane, QLD 4000, Australia

ARTICLE INFO

Article history:
Received 28 August 2014
Received in revised form 21 April 2015
Accepted 18 May 2015
Available online 23 May 2015

Keywords:
Early deformation
Thrusting
Structural control
Gold mineralization
Yilgarn Craton

ABSTRACT

The earliest pervasive deformation events in the Archaean Eastern Goldfields Superterrane of the Yilgarn Craton are partly obscured by subsequent deformation and pre-date rocks exposed over large areas. As a result, uncertainty exists about the nature, timing and role that early deformation events played in controlling regional architecture and gold mineralization in this world-class metallogenic province. The Daisy Milano mining camp in the southern Kurnalpi Terrane has opened up new exposures in relatively old geological sequences, which record structures that pre-date the main ENE-WSW D_2 shortening event. These D_1 structures represent the earliest pervasive deformation events in the Eastern Goldfields Superterrane and are characterized by a pervasive bedding-parallel foliation ($S_1//S_0$) that accommodated NW-verging thrusting. The same foliation planes also accommodated normal movement verging to the SE, interpreted to indicate periods of stress relaxation. Alternatively, thrusting and normal movement could have been contemporaneous, defining a pure shear event. D_1 structures are overprinted by steeply dipping, NNW-striking foliation planes that are axial planar to folds and local crenulation cleavage (F_2 folds). This second foliation is parallel to and overprints post-D_1, sub-vertical, plagioclase-phyric tonalite dikes, at the margins of which the Daisy Milano gold deposits formed. Deposits occur stratigraphically below moderately SW-dipping ultramafic layers that are sub-parallel to the early thrust foliation and acted as impermeable caps to mineralizing fluids. Mineralization occurs also in NE-SW to ENE-WSW quartz veins in the hinge zones of open and gently plunging F_2 folds in a competent dolerite sill. Mineralization was either synchronous with or post-dated D_2. Two samples of tonalite dikes at Daisy Milano were analyzed using zircon LA-ICP-MS U–Pb geochronology and yielded ages of 2687 ± 7 Ma and 2676 ± 9 Ma, placing an upper bound on the timing of D_2 and gold mineralization at Daisy Milano, and a lower bound on the timing of D_1.

1. Introduction

The concentration of orogenic "lode" gold deposits in the Eastern Goldfields Superterrane in the Yilgarn Craton has led to considerable efforts in understanding the nature, history and geometry of its rock sequences. Gold mineralization is controlled by structures, as well as lithological and structural complexity, which create the necessary conditions for focusing migration of mineralizing fluids (Davis et al., 2010; Hodkiewicz et al., 2005; Weinberg et al., 2004). The relative timing between mineralization and structural evolution of the Eastern Goldfields Superterrane has been a matter of great interest and debate. While many deposits may have been formed late in the structural evolution (Davis et al., 2001; Groves et al., 2000), there is evidence for protracted mineralization (Bateman et al., 2001; Bucci et al., 2004; Davis et al., 2010; Davis and Maidens, 2003; Witt, 2001). Weinberg and van der Borgh (2008) have argued that some small deposits in the region of Leonora were associated with the earliest, D_1, and the latest, D_5, extensional events. In any case, early structures played a significant direct or indirect role in controlling gold deposition (e.g., Miller et al., 2010). However, little is known about the nature of the earliest structures because of overprinting by later deformation, or because it is simply not recorded by the younger rocks exposed.

The nature of the first deformation event, D_1, has proven to be elusive and has been used to include any structure that pre-dates the well-developed ENE-WSW shortening D_2 event. The southern part of the Kurnalpi Terrane (Fig. 1) is composed of rock sequences ranging in age from 2720 to 2690 Ma (Barley et al., 2008). These

* Corresponding author at: School of Earth, Atmosphere & Environment, Monash University, Building 28, Wellington Road, Clayton, VIC 3800, Australia. Tel.: +61 3 9905 4902; fax: +61 3 9905 4903.
E-mail address: Roberto.Weinberg@monash.edu (R.F. Weinberg).

http://dx.doi.org/10.1016/j.precamres.2015.05.013
0301-9268/

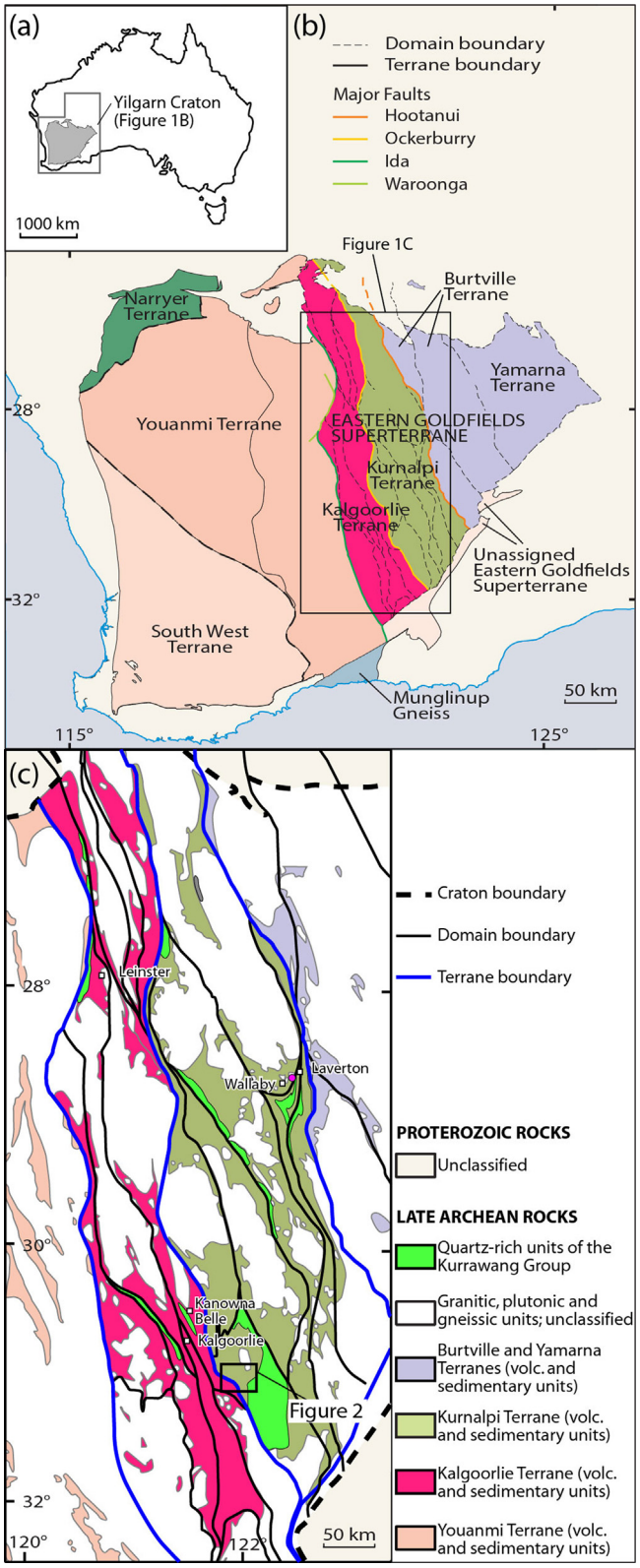

Fig. 1. Simplified geological maps of the basement rocks in the Yilgarn Craton, Western Australia. (a) Location of Yilgarn Craton in Australia. (b) Location of Kalgoorlie, Kurnalpi, Burtville, and Yamarna Terranes of the Eastern Goldfields Superterrane in the eastern Yilgarn Craton. (c) Simplified geological map of the Kalgoorlie and Kurnalpi Terranes. The location of Fig. 2 is shown. Figures modified after McGoldrick et al. (2013).

are relatively old compared to rocks exposed in the better known Kalgoorlie Terrane to the west. Recent open-cut mining in the Daisy Milano mining camp in the Kurnalpi Terrane provides an opportunity to access quality exposures and drill cores recording early structures. We start this paper with a brief summary of the current views on the structural evolution of the Eastern Goldfields Superterrane and a short description of the geology of the Kurnalpi Terrane and of the mining camp. This is followed by a structural study of the mining camp. We number the structures described according to their local overprinting relationships, and subsequently discuss their link to the regional deformation events. We then present U–Pb zircon dating results of two tonalite intrusions dikes and use the results to bracket the timing of D_1 and gold mineralization.

2. Regional geology

2.1. Structural evolution

Earlier work divided deformation in the Eastern Goldfields Superterrane into four main crustal shortening phases, D_1–D_4 (e.g., Swager, 1997; Weinberg et al., 2003b; Witt and Swager, 1989), and more recently other deformation events have been added, modifying this early framework to account for more detailed data and to include extensional events (e.g., Blewett et al., 2010; Czarnota et al., 2010; Weinberg and van der Borgh, 2008). As summarized in Blewett et al. (2010), major extension occurred during basin development and deposition of the greenstone sequences in the Eastern Goldfields between 2720 Ma and 2670 Ma (e.g., Groves and Batt, 1984; Hammond and Nisbet, 1992; Miller et al., 2010; Squire et al., 2010; Swager and Griffin, 1990; Swager, 1997; Williams and Currie, 1993; Williams et al., 1989; Williams and Whitaker, 1993). This extensional event is thought to control the broad NNW-trending grain of the region (Blewett et al., 2010), but just how these earliest structures are inferred and interpreted remains ambiguous (Miller et al., 2010).

In the central-northern part of the Kalgoorlie Terrane, D_1 has been described as an extensional phase of isoclinal recumbent folding and subhorizontal nappe-type movement (Archibald et al., 1978; Martyn, 1987; Williams and Currie, 1993). Passchier (1994) described a poly-directional extensional event related to the development of early recumbent folds. High-grade granitic domes were interpreted as early metamorphic core complexes developed during extension and post-dating greenstone deposition (Williams and Whitaker, 1993). Foliations at the outer margins of one such dome close to Leonora, in the central-northern part of the Kalgoorlie Terrane, have radial, down-dip lineation and record normal movement indicative of granite dome exhumation in relation to the surrounding greenstone sequence (Weinberg and van der Borgh, 2008). Structures in this area were interpreted by these authors to result from poly-directional extension, contemporaneous with granite doming rather than a metamorphic core complex (Williams and Currie, 1993), which is typically associated with uni-directional extension.

As noted by Swager (1997), evidence for early extension in the southern part of the Kalgoorlie Terrane is ambiguous, although he accepted that extension may have preceded the first major shortening D_1 event that he and others documented. D_1 shortening south of Kalgoorlie is characterized by major north-verging thrusting (Knight et al., 1993; Martyn, 1987; Swager and Griffin, 1990; Witt and Swager, 1989) leading to regional scale recumbent folds and repetition of the stratigraphy (Martyn, 1987; Swager, 1997). Martyn (1987) suggested that most, if not all contacts between mafic–ultramafic assemblages and felsic volcanic-sedimentary suites in the Mount Hunt area south of

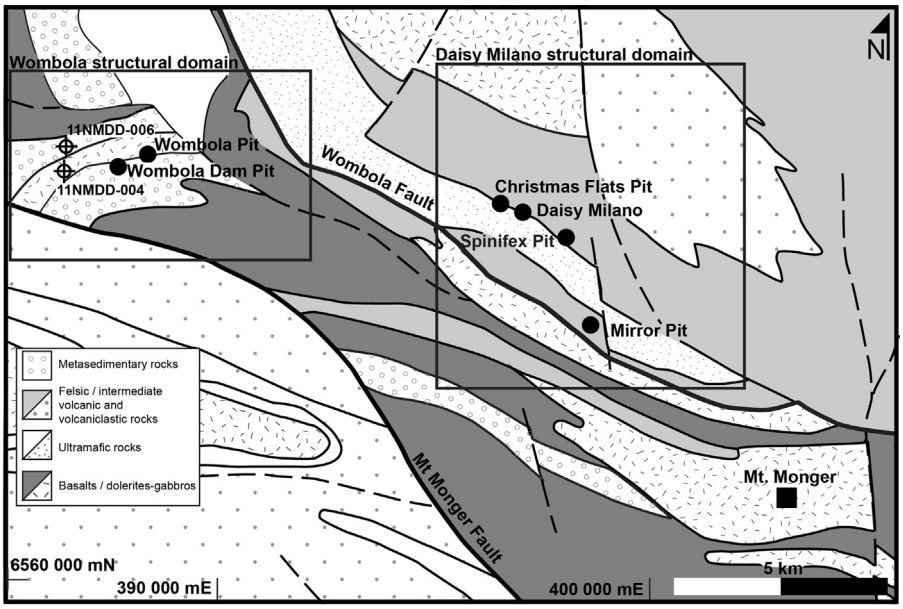

Fig. 2. Geological map of Mount Monger region including the Daisy Milano mining camp, based on 1:500,000 map of the Geological Survey of Western Australia (GSWA, 2008), with additional input from Swager (1997) and from Daisy Milano geologists. Thick line indicates the Mt Monger fault marking the boundary between the Kurnalpi Terrane to the east and the Kalgoorlie Terrane to the west. Localities, pits and position of collars of drillcores mentioned in text are marked.

Kalgoorlie are faulted and sheared, noting that the similarity between different mafic–ultramafic volcanic units separated by felsic volcanic rocks 'is more consistent with structural repetition than with the less likely re-establishment of identical volcanic conditions after a long interval of felsic volcanisms and sedimentation'. Swager (1997) summarized the D_1 event in the Eastern Goldfields as a north-directed thrust-stacking deformation giving rise to north-verging recumbent folds, pre-dating a possible extensional event inferred from seismic studies.

These early events were followed by a polyphase history of deformation, starting with a regional ENE-WSW contraction event, known as D_2, the major fabric-forming event across the Eastern Goldfields (Blewett et al., 2010; Platt et al., 1978; Swager, 1997; Witt and Swager, 1989). This event is responsible for major upright, doubly-plunging, north-northwest-trending folds, the regional steep foliation and the reactivation of pre-existing domain/terrane boundary faults and associated structures (Swager, 1997; Weinberg et al., 2003a). It folded D_1 thrusts and sedimentary sequences, such as the Kurrawang Group in the Kalgoorlie Terrane (dated to 2658–2655 Ma, Squire et al., 2010). After this event, the region underwent other deformation events and there remains significant uncertainties about their nature and how they relate to each other from place to place (Blewett et al., 2010; Czarnota et al., 2010; Weinberg and van der Borgh, 2008; Witt and Swager, 1989). Most significantly, some of these later events were responsible for the development of the large-scale strike-slip shear zones that characterize the Eastern Goldfields (Blewett et al., 2010; Morey et al., 2007; Weinberg et al., 2005).

The early structural evolution summarized above has been recently challenged by Blewett et al. (2010), who argued that komatiite units are ambiguous stratigraphic markers and may not imply thrust stacking. This is because geochronological data suggest that some komatiite have different ages (Barley et al., 2002) and some may in fact be intrusive (Trofimovs et al., 2004). Furthermore, structures in the southern nose of the Scotia-Kanowna dome close to Kalgoorlie, used by Swager (1997) in support of thrust stacking, have been shown to be younger than the regional ENE-WSW D_2 shortening. Recent detailed structural work in the Kanowna Belle deposit, on the nose of this dome, determined that the first two local deformation phases (local D_1 and D_2) were related to NW-directed thrusting (Davis et al., 2010). These structures were overprinted by a local D_3 characterized by ENE-WSW flattening. Using detailed age dating, Davis et al. (2010) demonstrated that the first deformation at Kanowna Belle affects rocks younger than 2656 ± 10 Ma, thus post-dating the regional D_2 contraction. This event is constrained by a number of syn-D_2 granitic intrusions with ages of ~2670–2655 Ma (Blewett et al., 2010). This lead Davis et al. (2010) to interpret the earliest events recorded at Kanowna Belle as related to the regional D_{4b} and D_5 of Blewett et al. (2010), in contrast to earlier interpretations that linked these structures to the earliest regional D_1.

Relevant here is that Czarnota et al. (2010) observed that D_2 folds affected the youngest volcanic successions across the Eastern Goldfields but did not affect the unconformably overlying late-basin sedimentary successions (such as the Kurrawang Group of Squire et al., 2010). Because the age of these unconformable units varies, D_2 was interpreted to be diachronous across the Eastern Goldfields: from ~2675 to 2665 Ma in the Kurnalpi Terrane in the east, and from ~2665 to <2660 Ma in the Kalgoorlie Terrane to the west (Czarnota et al., 2010).

In this paper we investigate the earliest structures preserved in the Daisy Milano mining camp of the Kurnalpi Terrane (Fig. 1; Cassidy et al., 2006). Rocks exposed are generally older than 2675 Ma and structures pre-dating the regional D_2 are well-preserved.

2.2. Kurnalpi Terrane

The Daisy Milano mining camp is part of the Bulong Domain of the southern Kurnalpi Terrane (Fig. 1; see Cassidy et al., 2006, for terrane divisions). Most of the literature on the Eastern Goldfields concerns the Kalgoorlie Terrane, but both terranes had similar deformation history (Blewett and Czarnota, 2007; Swager, 1997). The rock successions of the Kurnalpi Terrane are broadly divided into two sequences: the intermediate (andesitic) to felsic Kurnalpi Sequence at the base (2715 ± 5 Ma to 2702 ± 5 Ma, based on SHRIMP age data from detrital zircons in Barley et al., 2008), which

has no obvious stratigraphic equivalent in the Kalgoorlie Terrane, and the mafic-ultramafic Minerie Sequence above it (2698 ± 3 Ma, based on the weighted mean of four felsic volcaniclastic samples, Barley et al., 2008), which has numerous mafic units and corresponds to the Kambalda Sequence in the Kalgoorlie Terrane. The Kurnalpi Sequence has been interpreted to be conformably overlain by the Minerie Sequence (Hickman, 1986; Barley et al., 2008) or tectonically interleaved with it, at least in the Bulong Domain (Barley et al., 2008). These two sequences have been intruded by felsic porphyries occurring as dikes and sills closely associated with mineralization at Daisy Milano (Hickman, 1986).

Despite some broad similarities in the stratigraphy of the Kurnalpi and Karlgoorlie Terranes, the former is distinguished by the presence of iron-rich sedimentary units (locally referred to as banded iron formations, BIF), generally smaller volumes of komatiites, and abundant andesite in dominant calc-alkaline complexes, underlying mafic and ultramafic units (Fig. 1; Barley et al., 2002, 2008).

2.3. Daisy Milano mining camp

The Daisy Milano mining camp is located in the Mt Monger region, on the SW flank of the Bulong Dome, a large NNW-trending and doubly-plunging anticline with outward-dipping greenstone successions and a granitic core. The Juglah Monzogranite forms part of the core of the Bulong Dome and has been dated to 2635 ± 4 Ma (Dunphy et al., 2003). In the Mt Monger region, the greenstone successions are dominated by the Kurnalpi Sequence: felsic to intermediate volcanic rocks and coarse volcaniclastic sediment with subordinate lava flows (Griffin and Hickman, 1988; Hickman, 1986). Graded bedding indicating younging to the southwest was identified in a creek 500 m from Mt Monger Station (Hickman, 1986). This volcanic succession is interpreted to be at least 3.2 km thick. This was calculated based on the horizontal distance from the lowest part of the felsic volcanic succession to the first occurrence of mafic rocks to the southwest (GSWA, 2008), assuming a 45° southwest dip of bedding (Hickman, 1986; Fig. 2). The metamorphic grade of the rocks is interpreted to be upper prehnite-pumpellyite to lower greenschist facies (Hickman, 1986).

Bedding in the Daisy Milano region generally trends WNW-ESE, dips about 45° to the SSW and has a NW-SE to NNW-SSE trending and steeply SW-dipping foliation. This foliation corresponds to the S_2 of Swager (1997), who interpreted the regional anticline associated the Bulong Dome to be part of his D_2. Neither older foliations nor evidence for major stratigraphic repetition by isoclinal folding or thrust faults were found. NW-SE to N-S shear zones were used to explain local geological discrepancies such as the 1 km effective dextral displacement of lithologies to the east of Mt Monger Station (Hickman, 1986).

The architecture and evolution of the Bulong Dome is strikingly similar to other major domes in the Kalgoorlie Terrane, such as the Scotia-Kanowna Dome (Davis et al., 2010). The major domes are NNW-trending, have doubly-plunging antiforms and large granitic cores that are flanked by outward-dipping late Archaean successions. Furthermore, many of the major structures associated with the late Archaean successions were formed contemporaneously with growth and development of domes. However, the stratigraphic units flanking the southern margin of the Bulong Dome correlate with units of the Kalgoorlie sequence, which were emplaced prior to about 2680 Ma. In contrast, the stratigraphic units flanking the southern margin of the Scotia-Kanowna Dome comprise successions of the late Black Flag Group and Merougil Group, deposited between about 2670 and 2658 Ma (Davis et al., 2010; Squire et al., 2010). The exposure of these older rock sequences on the southern flanks of the Bulong Dome provides a valuable record of the early deformational history.

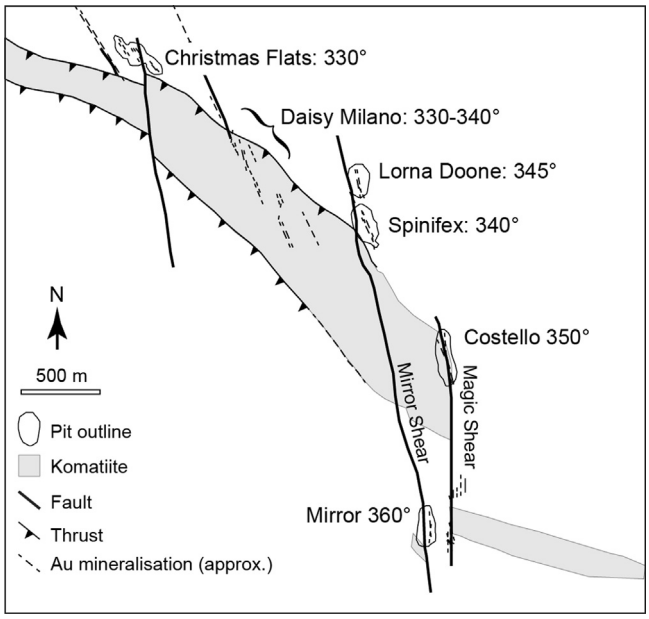

Fig. 3. Simplified map of gold deposits in the Daisy Milano domain showing orientation of mineralized structures. At Daisy Milano, mineralization is underground, underneath the ultramafic layer which dips ~45° SE. Orientation of mineralization given beside each main deposit rotates from 330° at Christmas Flats Pit in the NW, to 360° Mirror Pit on the shear zone offsetting komatiite unit in SE. Map based on information from Silver Lake Resources.

The Daisy Milano mining camp has been divided into two structural domains: the Daisy Milano domain to the east of the Wombola Fault, and the Wombola domain to the west (Fig. 2). The Daisy Milano domain is characterized by lithological contacts trending NE-SW and shear zones trending NNW-SSE (Fig. 1; Jones, 2007). It is also cross-cut by a N-S trending dextral fault with a displacement of ~750 m (Figs. 2 and 3; GSWA, 2008). The main lithofacies identified in this domain are komatiite, pillowed andesite, andesite breccia, volcaniclastic rocks, including monomictic and polymictic conglomerates and sandstones of intermediate composition, basalt, plagioclase-quartz dacite porphyry intrusions, and some later intrusions including a possible lamprophyre and E-W Proterozoic dolerite dikes. The age of the volcaniclastic rocks is similar to that of the komatiite, according to two samples of andesitic feldspathic sandstones from near Mt Monger, dated to 2702 ± 5 Ma and 2708 ± 5 Ma (Barley et al., 2002), and komatiite at the Bulong Townsite, dated to 2705 ± 4 (Nelson, 1997).

The Wombola domain has contacts trending E-W, contrasting with the NW-SE trend in the Daisy Milano domain (Fig. 2), and to most of the Eastern Goldfields where contacts trend NNW-SSE. The domain comprises an ultramafic unit in the east, overlain by a sedimentary sequence that youngs to the south, interlayered with subordinate andesite and basalt (Jones, 2007). In the west, the ~150 m thick mineralized Wombola Dolerite sill intrudes a sedimentary sequence composed of siltstone, quartzo-feldspathic sandstone, shale and chert (Jones, 2007). This western sequence may represent a younger part of the same stratigraphy exposed further east investigated by Jones (2007). Two sets of mineralized quartz veins cross-cut this stratigraphy: one set trending 055–060° and dipping steeply NW, and the other trending E-W and dipping steeply N or S.

The Wombola domain is bounded to the west by the Mt Monger Fault, and to the east by the Wombola Fault. Jones (2007) found that it records two deformation phases, which she linked to the regional D_1 and D_2 defined by Swager (1997): an initial thrusting event to the north, followed by an ENE-WSW crustal shortening event, giving rise to upright NNW-trending folds. Thrusting to the

north is characterized by bedding-parallel shear zones and gently dipping shear zones at the contacts of the dolerite sill, and tight folds with SW-plunging fold axes parallel to a stretching lineation (Jones, 2007). These structures are overprinted by open F_2 folds with hinges spaced by hundreds of metres. These folds are associated with a weak penetrative axial-planar foliation trending N to NW and steeply dipping, which intersect the bedding-parallel S_1 foliation, resulting in a moderately S- to SE-plunging intersection lineation (Jones, 2007). Furthermore, gently-dipping D_1 thrusts are consistently offset by anastomosing, NW-trending, NE-dipping sinistral faults, interpreted as belonging to D_2. The results presented here confirm and expand on these interpretations.

3. Daisy Milano domain

The Daisy Milano domain, east of the Wombola Fault, encompasses a number of gold deposits (Figs. 2 and 3). The open-cut pit at Christmas Flats best records the overprinting relationship between D_1 and D_2 structures, whereas the pit at Mirror best records the complex nature of D_1. The Lorna Doone, Spinifex, and Costello pits, as well as the Daisy Milano underground mine further confirm the nature of deformation events.

3.1. Christmas Flats Pit

The Christmas Flats Pit lies above the Daisy Milano underground mine (Fig. 4). The pit has three lobes (inset on top right of Fig. 4a) and each lobe follows steeply W-dipping, NNW-trending porphyritic dikes of tonalitic composition, that intruded a sequence of volcaniclastic sandstone, polymictic conglomerate (containing dacitic and basaltic clasts) and andesite, metamorphosed to chlorite schist. The sequence is overlain by pillow basalt and komatiite, exposed at the southern end of the pit, with bedding-parallel contact dipping 45° SW. Gold mineralization is hosted by narrow quartz veins in chlorite schist (intermediate meta-volcanic rocks) at the boundaries of the dikes (Fig. 5) where they contain 2–30 g/t of gold. Extensional low-angle veins within the dikes may contain up to 1 g/t of gold and the tonalite itself contains <0.5 g/t.

The country rock to the mineralized dikes has two foliations: a gently SW-dipping S_1 foliation and a steeply WSW-dipping S_2 foliation (Fig. 4b). S_1 is parallel to bedding (300°/45° W) and rotates and steepens towards the dike, making it difficult to distinguish from S_2 (Fig. 4b). In places, S_1 is crenulated by the steeply-dipping S_2, indicating their relative timing. S_2 is parallel to and becomes more intense in the vicinity of dikes, and is also parallel to the plane of flattening of clasts in the conglomerate. It lacks obvious shear sense indicators and has a lineation plunging moderately SSE (~160°/35°). These features suggest that S_2 is a result of a deformation event with a strong pure shear deformation. Significantly, only S_2 has been documented inside the dike.

A porphyritic dike in the central lobe of the Christmas Flats Pit is boudinaged (Fig. 5), with an apparent stretching direction near vertical and an apparent shortening direction orthogonal to the dike orientation and S_2. The S_2 foliation in the dike, the boudinage, quartz veining and mineralization inside and at the dike margins, all combined suggest that diking occurred either before or during D_2, and that mineralization occurred after dike emplacement, most likely during D_2, explaining gold-rich quartz veins in boudin necks.

3.2. Mirror Pit

The Mirror Pit is the southernmost mine in a group that is roughly aligned along the N-S trending Mirror shear zone, which hosts the ore and offsets the ultramafic komatiite body dextrally by ~750 m (Fig. 3). The main N-S shear zone is not currently exposed in the pit but was mapped by Westchester Mining (Westchester, 1993) and interpreted to continue northwards into the Lorna Doone and Spinifex Pits (Fig. 3).

The rocks exposed in the pit are a sequence of volcaniclastic sandstone and polymictic conglomerates of intermediate composition that have been metamorphosed to greenschist facies. Similar to Christmas Flats, the succession is overlain in the south of the pit by komatiite with a lower contact dipping 30–40° SW (Fig. 6), and intruded in the north of the pit by a tonalite sill (115°/29° SW). The sequence is cross-cut in the south by a pair of mafic dikes dipping moderately SW and another dipping steeply N.

Polymictic conglomerate interbedded with fine-grained sandstone layers define bedding, S_0, which is parallel to an S_1 foliation, and, like at Christmas Flats, dips ~40° to the S and SW. S_1 is accompanied by a well-defined stretching lineation, L_{st}, plunging 30° SSE. A steeply W-dipping S_2 foliation (155°/70° W) was measured in the pit walls. The bedding-parallel S_1 steepens and rotates towards parallelism with S_2 (compare stereonet insets in Figs. 6 and 4).

The major difference between Christmas Flats and Mirror Pits is that mineralization is hosted by S_2-parallel quartz veins at the margins of tonalitic dikes at Christmas Flats Pit, and in the N-S trending shear zone in the Mirror Pit. This shear zone is not exposed currently and may be responsible for a slight offset in foliation measurements on either side of the pit, bedding being steeper on the east compared to the west (Fig. 6 stereonet inset).

In the Mirror Pit, S_1 foliations have kinematic indicators that are not found at Christmas Flats. Large porphyritic dacitic clasts in the conglomerate, up to 30 cm in diameter, contain hornblende phenocrysts sheared into sigma-shaped grains and quartz grains with strain-shadows both consistently (i.e., over a number of different individual clasts) indicating top-to-NNW thrusting, parallel to L_{st} (Fig. 7a and b). Normal movement was also documented in a zone 10 m wide, where movement sense is defined by S–C fabric (Fig. 7c and d), with the C-plane and stretching lineations parallel to S_1 and L_{st}, respectively, measured in areas of reverse movement. The sections of the pit wall where normal and reverse movements were documented are shown in Fig. 6. Overprinting relationships between thrusting and normal movement were not identified.

3.3. Other pits

The Spinifex and Lorna Doone pits are located along the NNW- to N-trending mineralized Mirror shear zone, and the Costello Pit is located along the roughly parallel Magic shear zone (Fig. 3), which continues south where it hosts the yet unmined Magic gold prospect. In contrast to Mirror, the shear zones at Spinifex, Lorna Doone and Costello have been intruded by closely spaced, foliated porphyritic dikes, parallel to the main NNW-trending steep foliation. By analogy to the other pits, this foliation is interpreted to be S_2. A gently-dipping cleavage was also observed, but overprinting relationships could not be determined due to intense weathering. Gold in Spinifex and Lorna Doone deposits occurs in narrow, high-grade (up to 30 g/t), quartz veins along dike contacts. These quartz veins sometimes act as fault planes as indicated by slickenlines. One such fault surface at Lorna Doone had a lineation plunging 42° S, but shear sense indicators were inconclusive. Given the large scale dextral offset of lithologies in map view (Fig. 3), it is likely that this fault is dextral with a reverse movement component.

3.4. Daisy Milano underground mine

The Daisy Milano mine lies between the Christmas Flats and Lorna Doone Pits and contains several mineralized structures including the one which is also exposed in the Christmas Flats Pit. Gold is hosted in narrow quartz veins at or near contacts between NNW-trending porphyritic dikes and the surrounding andesite (Fig. 8a), which is either pillowed or brecciated. The sequence is

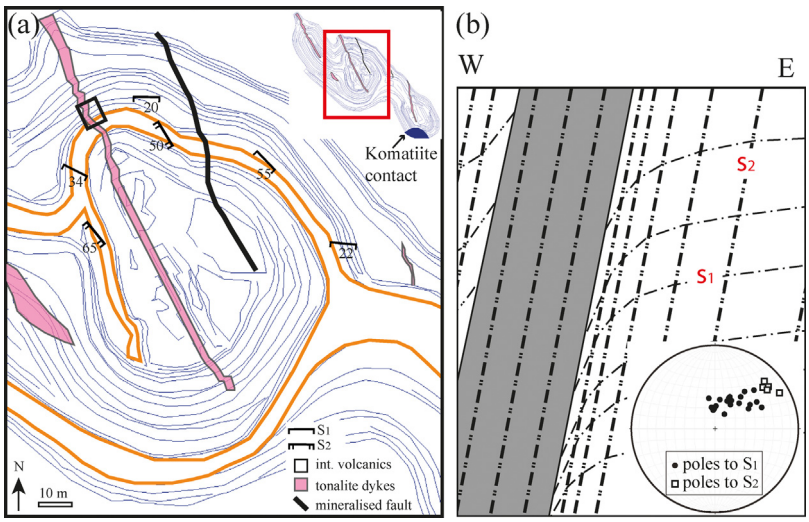

Fig. 4. (a) Central lobe of Christmas Flats Pit (ramp in orange). The main felsic porphyritic dikes (pink) are mineralized along contacts. Inset shows open pit outline and marks the central lobe. Small black rectangle marks location of exposure in (b) and in Fig. 5. (b) Schematic cross section of porphyry dike (grey) with dike-parallel steeply-dipping foliation (S_2) intensifying close to dike and causing steepening of gently-dipping foliation (S_1). This relationship was observed only on the east side of the dike due to lack of exposure on the west. Lower hemisphere, equal-area stereonet projection shows poles to both foliations and records rotation and steepening of S_1 towards S_2. (For interpretation of the references to color in this figure legend, the reader is referred to the web version of this article.)

faulted by two main brittle NW-trending faults dipping moderately SW, and cross-cut by moderately N-dipping tourmaline-bearing quartz veins, post-dating gold mineralization (and also found in the Lorna Doone Pit). Gold-bearing quartz veins are usually steeply-dipping WSW, parallel to the dikes but sometimes dip more gently near faults. These quartz veins are typically very narrow (<1 cm to 5 cm) and can define ptygmatic folds within porphyritic dikes. The ore-shoot in the mine plunges moderately to SE.

4. Wombola Domain

4.1. Wombola Dam oriented core

Two oriented diamond drill cores from the Wombola domain (Fig. 2) were studied: 11NMDD-004 (386,491 mE, 6,569,318 mN; plunging 55°–120°), 1.1 km west of Wombola Dam Pit, and 11NMDD-006 (386,536 mE, 6,569,907 mN; plunging 60°–325°) 1.1 km northwest of Wombola Dam Pit.

Drillhole 11NMDD-004 is 250 m long through the Wombola Dolerite. It comprises mainly biotite-amphibole schist, interbedded with metapelites and intruded by plagioclase-porphyry tonalite sills. Most of the figures in this sub-section and most of the structural measurements in Fig. 9 come from this core. Additional structural measurements are from 11NMDD-006. Attitudes of structures in the original sequence were calculated by measuring α, β and γ angles in the oriented drillcore and converting them to true strike, dip and plunge using the methods of Holcombe (2014).

4.1.1. Foliation, lineations and shear sense

A single foliation is recorded in the two oriented cores. This is a bedding-parallel foliation overprinting all lithologies, including the intrusive tonalitic sill, that is associated with a stretching lineation, L_{st}, and defines centimetric-folds with a fold axis, L_f, perpendicular to L_{st} (Fig. 9). The main foliation dips gently in a spread of directions, whereas the stretching lineations, L_{st}, are restricted to the NW and SE quadrants, depending on the dip of S_1. Fold axes, L_f, always plunge gently (subhorizontally) to the SW (Fig. 9). Several types of kinematic indicators such as S–C fabric, sigma-shaped clasts, microfaulting and fold-and-thrust planes were documented, in over 20 locations along the core (Figs. 10–12). They generally point to top-to-NW movement. In some sections of core, although top-to-SE shearing was found.

Under the microscope, a sample from a tonalitic sill, with plagioclase porphyroclasts up to 5 mm (typically 1–3 mm long), in

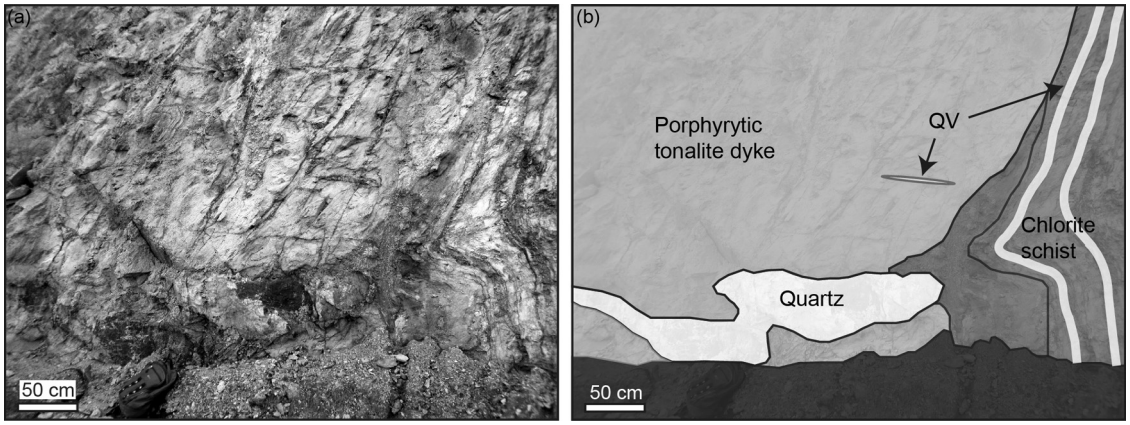

Fig. 5. (a) Photograph of a vertical wall with part of a 4-m-wide boudinaged porphyritic dike in Christmas Flats Pit. (b) Same as (a) marking the different rock types and highlighting folding of chlorite schist into the boudin neck, as well as a massive quartz vein in the boudin neck itself. Contact between dike and schist is mineralized. QV stands for quartz vein.

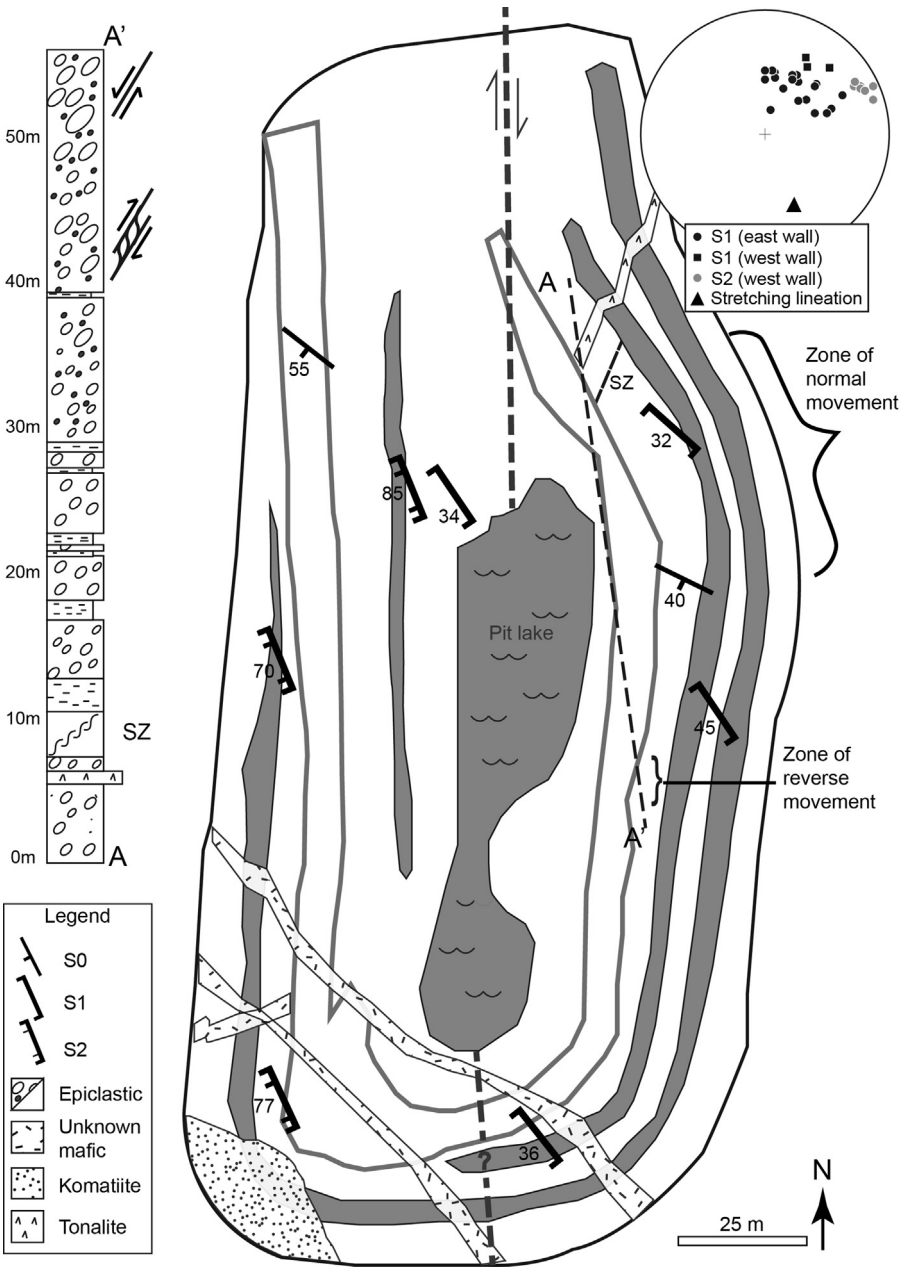

Fig. 6. Map of Mirror Pit indicating locations of normal and reverse movement. Exposures comprise an epiclastic sequence of both sandstones and polymictic conglomerates and overlying komatiite with minor mafic dikes and a felsic (tonalite) porphyry sill. Stratigraphic log on the left represents the A–A′ section line on east side of the pit where the two kinds of volcaniclastic rocks are differentiated. Dashed black line represents the location of inferred N-S shear zone based on previous pit mapping (VL, 2007; Westchester, 1993) and regional maps (GSWA, 2008). North end of the pit is back-filled, and the shear zone was not found on south wall. Representative foliations are shown in map and equal-area, southern hemisphere stereonet plots poles of all S_1 and S_2 measured. Note similarity to stereonet from Christmas Flat. Grey bands are flat burms, uncoloured bands are steep walls.

a groundmass of quartz and biotite, shows strain shadows with asymmetry indicating top-to-NW shear sense (Fig. 11). There are also many symmetric strain shadows indicating a pure shear component. In contrast, samples from the mafic Wombola Dolerite unit, predominantly made up of amphibole-quartz-plagioclase-biotite, display evidence of top-to-SE movement (Fig. 12). Both shear senses are associated to the same stretching lineation, L_{st} (stereonet in Fig. 9).

4.1.2. Boudins

The same drillcore records boudinage of mineral grains and clusters in the Wombola Dolerite. Boudinage is along the S_1 fabric with a NW-SE maximum stretching direction parallel to L_{st}. Sections perpendicular to S_1 and parallel to the stretching lineation, L_{st}, typically show symmetric boudinage of amphiboles and extensional fractures within grains. Boudin necks are filled in by quartz and sometimes pyrite. The boudin neck axis, L_b, is parallel to the fold axis, L_f, and perpendicular to L_{st} (Fig. 13).

4.2. Wombola Dam Pit and surrounding outcrops

The Wombola Dam Pit is elongated NW-SE so as to intersect a number of steeply NW-dipping mineralized quartz veins cutting through the Wombola Dolerite (Fig. 14). The gently-dipping S_1 foliation described in the core above, drilled just 1.1 km to the west of the mine, is also prominent in the pit (Fig. 15). In the pit, the dolerite has a foliation parallel to its contact with the sedimentary rock exposed at the southern edge of the pit, and parallel to

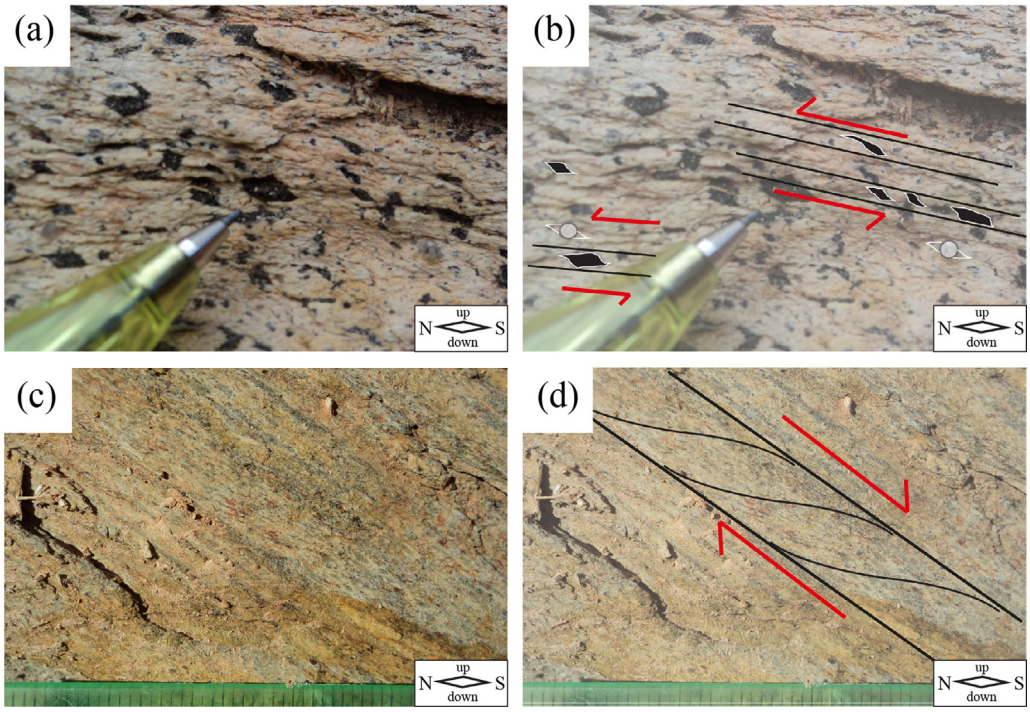

Fig. 7. (a) Sigma-shaped hornblende grains and strain shadows around quartz grains indicate top-to-NW sense of shear. The vertical plane of the photo is parallel to stretching lineation, L_{st}, and perpendicular to foliation. (b) Same as (a) with interpretation lines. (c) Normal shearing defined by S–C fabric indicative of top-to-SE on the same shear plane, C, as thrusting in (a). (d) Same as (c) with interpretation lines. Hatched lines on the ruler are millimetres.

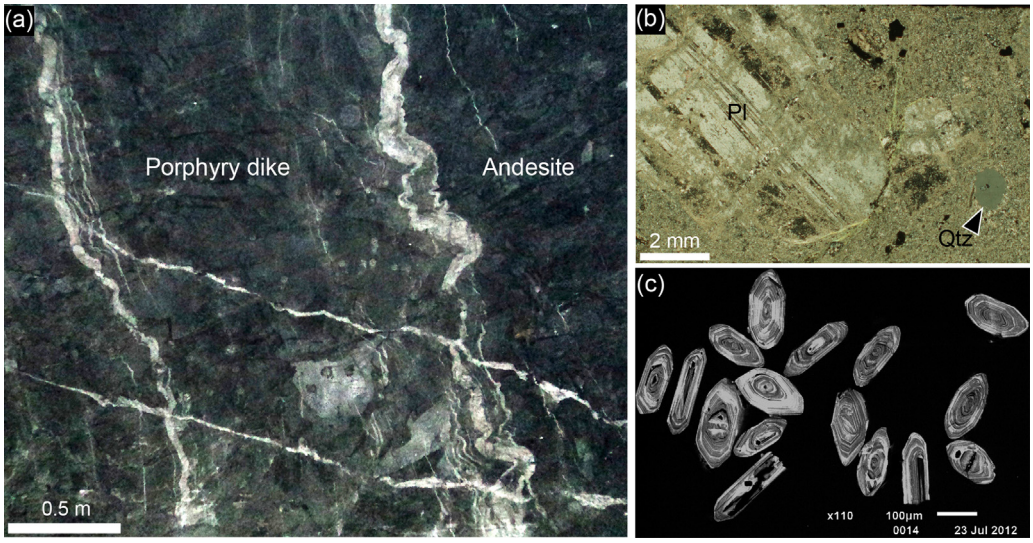

Fig. 8. (a) Porphyry dike in Daisy Milano underground mine cutting through andesite with multiple, parallel quartz veins at the contact including some ptygmatic ones; (b) photomicrograph of weakly seriticised plagioclase phenocryst, and a rounded quartz grain and minor opaque minerals in aphanitic quartzofeldspathic matrix, now mostly calcite and sericite. Cross-polarized light; (c) representative subset of zircons from sample LC-75 in cathodoluminescence under scanning electron microscope (SEM) showing magmatic zoning and growth patterns.

bedding in these rocks. Foliations measured in the pit walls dip gently away from the centre of the pit and define a large-scale, open fold with an axis plunging gently to the SE (stereonet in Fig. 14). Foliation planes found in exploration trenches 100 m north of the pit define a fold plunging gently to the NW (Fig. 14). The combination of the data-sets from the pit and nearby trenches suggests weakly non-cylindrical folds, possibly NW-SE doubly-plunging.

Bedding measurements from surrounding outcrops provide further evidence of a second deformation event causing folding. A ridge of silicified sedimentary rock 450 m SE of the Wombola Pit has folded bedding with a wavelength of 2 m, a NNW-striking, WSW-dipping axial-planar spaced cleavage, S_2, overprinting the folded bedding-parallel S_1 foliation. We attribute this deformation to the regional D_2 event because S_2 overprints the early low-angle deformation and because of its upright NW-SE or NNW-SSE axial plane (see also Jones, 2007).

Gold-bearing quartz veins cross-cut the Wombola domain trending broadly NE-SW (Fig. 16). They vary in width from a few cm to 40 cm. The veins may be separated into two groups based on their attitudes and intersections: (a) NE-trending veins from the Wombola Dam Pit, intersecting along a line plunging steeply

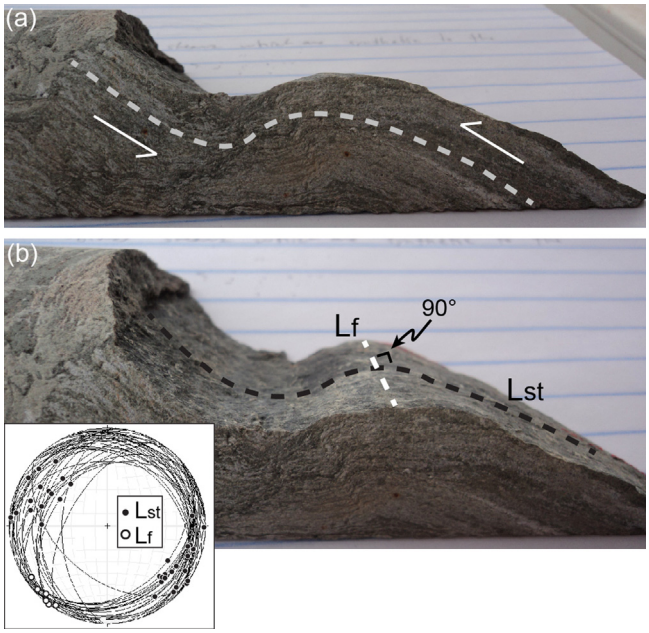

Fig. 9. Wombola Dolerite from core 11NMDD-004 at 140 m. (a) Gently dipping foliation defining asymmetric fold with NW vergence. (b) Same as (a) at a different angle, showing stretching lineation, L_{st} (black dashed line), on curved S_1 surface defining a fold with fold axis, L_f (white dashed line), perpendicular to L_{st} (stereonet inset). Note L_{st} undulates over the fold. Structures from drillcores 11NMDD-004 and 006 are plotted in equal-area southern hemisphere projection stereonet. Foliation dips gently, L_f plunges gently SW, and L_{st} plunges gently SE or NW. Spread of data may be due in part to errors in orientation line on the core.

N (Fig. 16a), and (b) ENE-trending veins from the Wombola Pit and various nearby trenches, dipping moderately to steeply to the N or S and intersecting along a line plunging gently WSW (Fig. 16b).

The intersection between quartz veins indicates the intermediate strain axis, *y*, at the time of emplacement. The two intersection lines in Fig. 16 are nearly 90° from each other and indicate a swap between the *y* and *z* strain axes between two groups of quartz veins. This is a common feature of many fracture zones that indicates switches between axes during fracturing. The NW-SE orientation of the broad upright antiform in the Wombola Dam Pit (Fig. 14) is consistent with the NE-SW shortening (*z* or *y*-axis in Fig. 16) and NW-SE extension (*x*-axis in Fig. 16) indicated by the veins. It is therefore possible that these auriferous quartz veins are the result of mineralizing fluid flow into dilational shear fractures developed as the competent dolerite body was being folded during D_2.

5. Geochronology

Two samples of the porphyritic tonalite were collected from the Daisy Milano underground mine at levels 19–50 and 35–52 (LC-75 and LC-77, respectively). Both samples are from the mineralized zone known as the Haoma structure and are interpreted to be from the same major intrusive unit. This intrusion generally trends NNW and dips steeply to the west parallel to the 330°/65° W foliation. Mineralized quartz veins commonly occur at the boundary between dikes and the andesite host rock (Fig. 8a)

The sampled tonalite is locally referred to as the 'Green Porphyry' (Fig. 8a) and contains about five modal percent plagioclase phenocrysts, up to 5 mm long, about one modal percent rounded quartz grains, up to 2 mm in diameter, and a quartzo-feldspathic groundmass (Fig. 8b). Zircons are present in the groundmass and are generally euhedral and elongate with well-defined crystal faces. Most zircons are between 100 and 150 μm in length, although rare crystals exceeding 200 μm are also present.

5.1. Method

Zircons were separated from the whole rocks at Monash University using standard heavy-liquid and electromagnetic techniques, then mounted and analyzed using a LA-ICP-MS at the Research School of Earth Sciences, The Australian National University. The sample preparation and analytical method used here is described in detail in Squire et al. (2010), who showed similar levels of accuracy and precision can be achieved for U–Pb geochronology of Neoarchaean detrital zircons using the SHRIMP and LA-ICP-MS methods. Standard zircons (TEMORA 2 and Plesovice) and NIST 610 glass were mounted with the unknown zircons, then cast in epoxy and polished to expose zircon interiors. Some 40 analyses (one analysis per grain) were performed for each of the samples using the LA-ICP-MS and all reported dates are based on $^{207}Pb/^{206}Pb$ (Appendix 1).

The method for processing the LA-ICP-MS data is similar to that described by Squire et al. (2010), but uses the IOLITE data reduction software (Paton et al., 2010). IOLITE incorporates two improvements not previously applied in LA-ICP-MS data processing: smoothing of the down hole average signal from the standard TEMORA 2 (the rough raw signal was used previously); and updated management of excess uncertainty evaluated against the TEMORA 2 primary standard (see below). Iolite also provides a simple visual utility for deciding what portion of a signal should be incorporated in the mean age for that ablation. These improvements result in a maximum age uncertainty (internal) of about 1% so no further exclusions are required on the basis of the noise in the resultant ablation period.

Concordance is taken to be agreement of the $^{207}Pb/^{206}Pb$ and $^{206}Pb/^{238}U$ ages within uncertainty, which includes a propagated uncertainty. Relative to internal (counting statistics) uncertainty, the propagated uncertainty is based on what term needs to be added to TEMORA 2 to get a population MSWD on TEMORA of 1.0. This extra term is a catch all for a series of uncertainty terms. Simply put, we assume the standard is a single age population and therefore with some ten or more analyses its MSWD should approach 1 if all errors are accounted for correctly. Therefore, expected and measured uncertainties should be about the same. In IOLITE this extra uncertainty is not a blanket term but is tied to the behaviour of the standards relative to the time of the analysis. Propagated uncertainty is not an external uncertainty term in our opinion, but a within-session term. Systematic uncertainties can affect session to session or lab to lab accuracy and we assume that minimum external uncertainty is a minimum of 1% (Allen and Campbell, 2012) which is what is quoted for the population $^{207}Pb/^{206}Pb$ ages.

All dates are reported as standard $^{207}Pb/^{206}Pb$ with no correction for common Pb. Concordia plots indicate that Pb loss is the main source of discordance. Because of high systemic Hg, we cannot measure a robust ^{204}Pb so must resort to a ^{208}Pb-based correction. The estimated common Pb as a percentage of the total ^{206}Pb ranges from 0.55 to −0.5% for LC-75, and from +0.8 to −1.2% for LC-77. A negative correction value indicates that the $^{208}Pb/^{232}Th$ age is somewhat younger than the $^{206}Pb/^{238}U$ age. It is important to note that correcting an age that is discordant because of Pb loss and not common Pb will result in spurious ages. To overcome this issue we use the ages deemed as concordant to gain a weighted mean average $^{207}Pb/^{206}Pb$ age, admitting that some Pb loss may be concealed within our measured uncertainty.

One feature not adopted from IOLITE was its calculation of ratio error correlation, which was calculated by fitting a line and r^2 for all ratios measured within a single ablation interval. Instead, we used the average bulk values which ensured positive results because ISOPLOT (Ludwig, 2003) only accepts positive ones. ISOPLOT was employed for Concordia plots and weighted mean calculations.

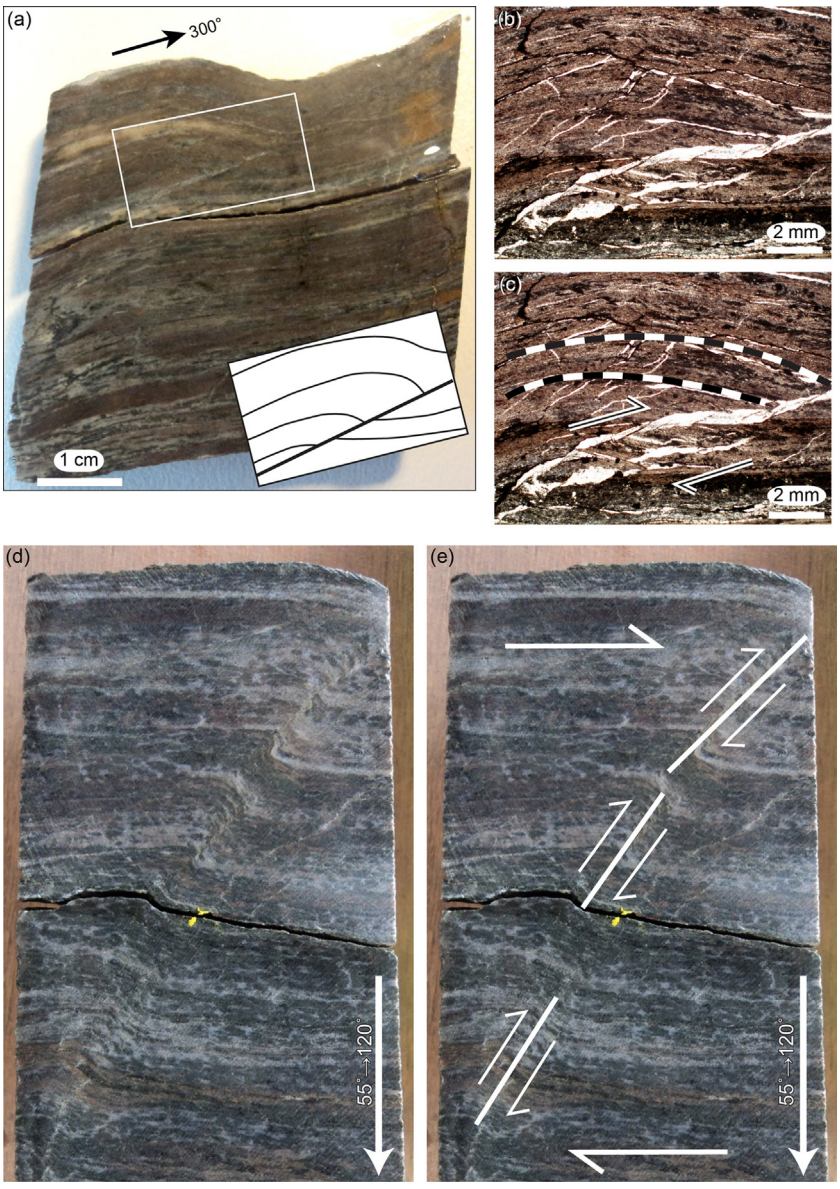

Fig. 10. Structures from core 11NMDD-004. Photographs taken perpendicular to foliation and parallel to stretching lineation, L_{st}. (a) At 87.6 m: NW-verging fold on a top-to-NW thrust-plane (arrow points NW). Frame marks position of the line drawing inset and photomicrographs (plane polarized light) in (b) which shows quartz infilling fracture spaces along thrust plane and in (c) with interpretation lines. Note that fold axis (perpendicular to the plane of view) is perpendicular to L_{st} (parallel to the page). (d and e) At 97.5 m: asymmetric folds on a thrust plane (dipping 20° to the SE) exhibiting top-to-NW thrusting. Fold axis, L_f, is perpendicular to the plane of view. Arrow on lower right marks the bottom of the core and points to 55° → 120°, down-plunge of the core; foliation dips 44° NW.

5.2. Results

5.2.1. Sample LC-75

Forty zircons were analyzed from this sample, of which 21 passed the above-mentioned selection criteria (Fig. 17a and b). Many of the outliers had anomalously high lanthanum, calcium or phosphorous, which is an indication of a non-zircon component and could negatively impact the accuracy of U–Pb data. Others were removed because they were discordant or had large uncertainties. A concordia plot for the robust zircon analyses shows a gross clustering of the data at about 2.7 Ga. Using propagated uncertainty, which averages 1% of the $^{207}Pb/^{206}Pb$ age, the 21 grains are deemed concordant and their weighted mean age is 2687 ± 7 Ma (MSWD = 1.2) (Fig. 17a and b). This result is interpreted to represent the igneous age of this sample.

5.2.2. Sample LC-77

Forty zircons were analyzed from this sample, of which 19 passed the above-mentioned selection criteria (Fig. 17c and d). The concordia plot for these data shows a gross clustering at about 2.7 Ga. Propagated uncertainties for $^{207}Pb/^{206}Pb$ ages average about 1%. Using these, 19 grains are concordant within error and rejecting one gives a weighted mean age of 2676 ± 9 Ma (MSWD of 2.6). This is interpreted as the igneous age of this sample.

6. Discussion

6.1. Nature of deformation

Across the Daisy Milano mining camp, the earliest deformation event is related to the development of the low-angle,

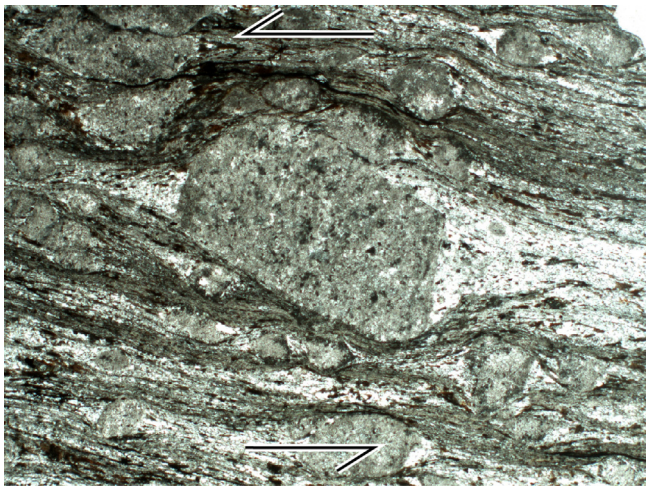

Fig. 11. Photomicrograph of tonalite intrusion from oriented core 11NMDD-004 at 83.3 m. Plagioclase strain-shadows indicate top-to-left (NW) sense of shear. Base of image is 11 mm long. Plane polarized light.

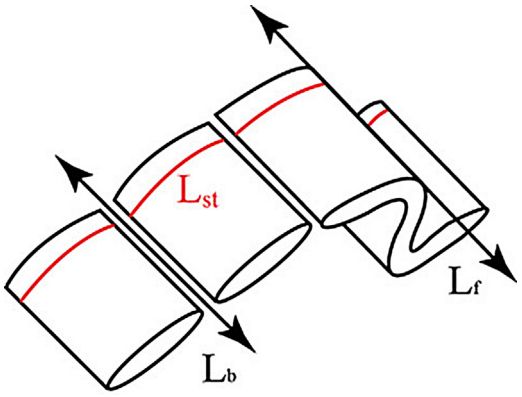

Fig. 13. Interpretative diagram showing the geometry of the folded and boudinaged S_1 fabric with boudin axis, L_b, parallel to fold axis, L_f, and perpendicular stretching lineation, L_{st}.

bedding-parallel foliation that trends E-W to NW-SE. This foliation has a stretching lineation that plunges SSE (Mirror Pit, Fig. 6) or is sub-horizontal trending NW-SE (drillcore 11NMDD-004, Fig. 9). The dominant movement direction inferred from shear sense indicators is top-to-NW thrusting, but there is also evidence for top-to-SE normal movement, on similar shear planes with similar transport direction, indicating local movement inversion (Figs. 6 and 9). $S_0//S_1$ undulates around SW-plunging F_1 fold axes (Fig. 9b), at right angles to the NW-SE stretching lineation, defining gentle folds, interpreted to be part of the same thrusting event. No evidence for the relative timing between the reverse and normal events was found and we refer to them as D_1 and D_{1e}. We interpret this early phase of deformation as a top-to-NW thrusting event, suggested by the dominance of thrusting shear sense indicators. In this case, top-to-SE normal movement marks periods of stress relaxation. Despite evidence for thrusting, we found no obvious high-strain zones at lithological contacts that could be interpreted as shear zones, and could not establish major stratigraphic repetition at the scale of the Daisy Milano camp. An alternate interpretation is that D_1 deformation was dominated by pure shear deformation, where top-to-NW and top-to-SE movements are contemporaneous and accommodate shortening perpendicular to S_1.

The steep, NNW-trending S_2 foliation overprints S_1 causing its rotation, crenulation or larger scale folding (e.g., Christmas Flats and Mirror Pits, Figs. 4 and 6). S_2 foliation is well-developed, dips ~75° WSW or steeper, and increases in intensity in the vicinity of NNW-trending felsic porphyry dikes in the Daisy Milano domain. D_2 is interpreted to be related with the large F_2 doubly-plunging NW-SE antiform at Wombola Dam Pit. This corresponds to the regional D_2 that elsewhere in the Kalgoorlie and Kurnalpi Terranes is associated with intense ENE-WSW contraction. The relatively low D_2 deformation intensity in the Daisy Milano mining camp is indicated at map scale by the trend of lithological contacts varying from E-W to NW-SE, rather than the regionally dominant NNW-SSE trend (Fig. 2). Preservation of D_1 structures could be related to the position of the mining camp on a D_2 strain shadow, on the south nose of the granite-cored Bulong Dome.

The N-S to NNW-SSE trending Magic and Mirror shear zones (Fig. 3) are both dextral (with a possible reverse component) and related to a number of deposits (Fig. 2, see also GSWA, 2008). Their kinematics is compatible with that of the late brittle faults that have affected the Eastern Goldfields (e.g., Blewett et al., 2010; Weinberg et al., 2005).

6.2. Timing of D_1

The low-angle S_1 foliation affects all volcano-sedimentary rocks of both the Kurnalpi and Minerie Sequences and therefore must be younger than the 2698 ± 3 Ma age for the greenstone

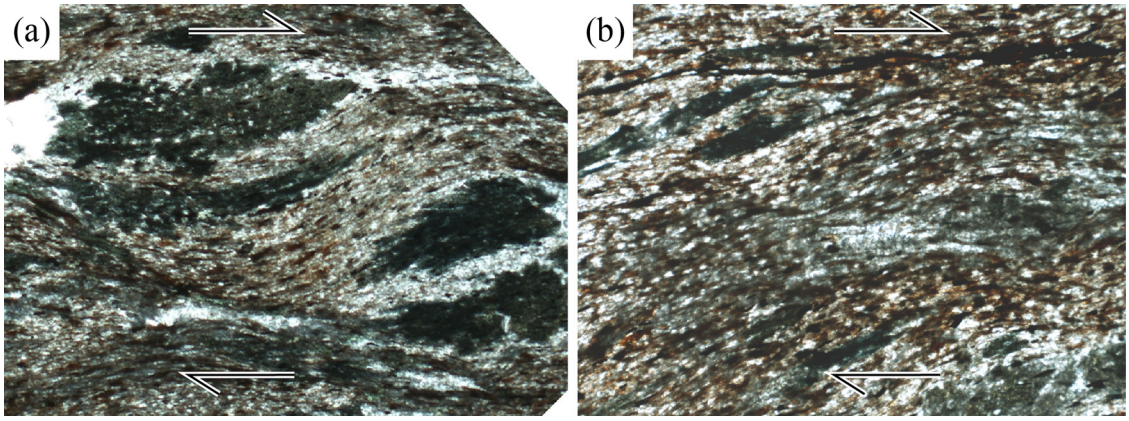

Fig. 12. Photomicrographs of oriented core 11NMDD-004 at 101.9 m, Wombola Dolerite. (a) S–C–C′ fabric indicating top-to-right (SE) shear sense. C is subhorizontal and C′ is diagonal from middle left to lower right. Photomicrograph shows amphibole porphyroblasts in a fine plagioclase-quartz-biotite ground mass. Base of image is 5 mm long. (b) S–C fabric indicating same shear sense. Base of image is 3 mm long. Plane polarized light.

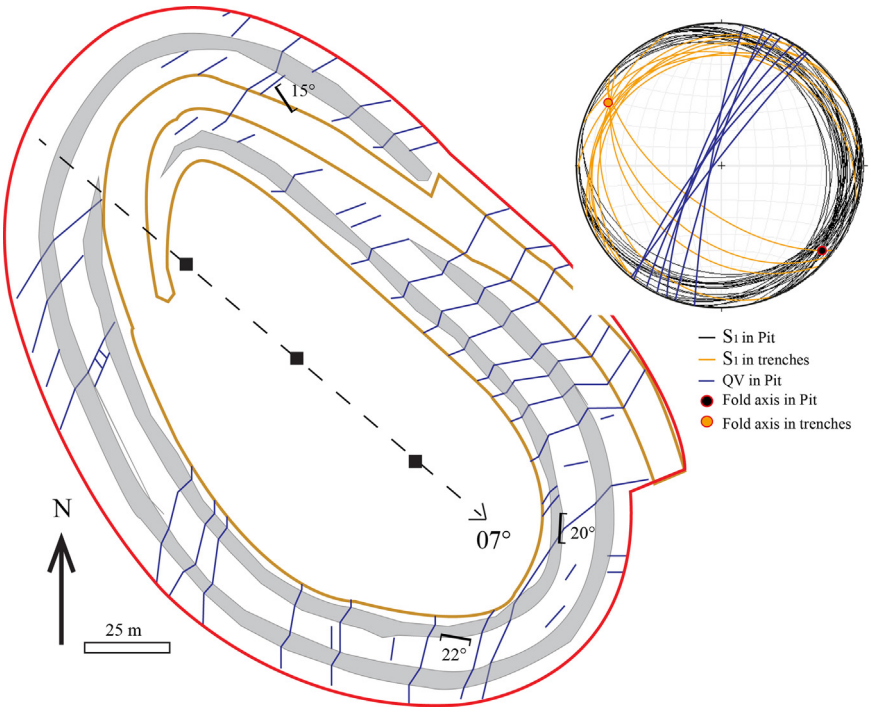

Fig. 14. Map of Wombola Dam Pit comprising almost entirely of Wombola Dolerite except for a sliver of overlying sedimentary rock in the SE edge (not shown). Average S_1 measurements of foliation in dolerite are given at three locations and define a broad gentle antiform with a gently-plunging fold axis to SE. Blue lines are steep mineralized quartz veins. Stereonet plots quartz veins (blue great circles trending NNE), S_1 foliation (black great circles) and those from nearby trenches to the north (orange great circles); equal-area, southern hemisphere projection. Grey bands on the rim represent flat burms whereas uncoloured parts are steep walls, outline (red), decline (brown), NE-SW-trending quartz veins (blue). (For interpretation of the references to color in this figure legend, the reader is referred to the web version of this article.)

successions of the Minerie Sequence (Barley et al., 2008). In drillcore 11NMDD-004, the felsic tonalite sill shows a pervasive S_1 foliation. In contrast, tonalite dikes with broadly similar composition, such as in the Christmas Flats Pit and Daisy Milano mine, only record S_2. These dikes have been dated here at 2687 ± 7 Ma and 2676 ± 9 Ma. These two ages are within error and merging the two data sets we obtain a single weighted mean aggregated age of 2681 ± 5 Ma, using ISOPLOT and its "automatic rejection" function, which culled two analyses.

We conclude therefore that D_1 started after 2698 ± 3 Ma (the age of the Minerie Sequence rocks) and ended before emplacement of the tonalite intrusions at 2681 ± 5 Ma. This interpretation is in direct contrast with the extensional event proposed by Blewett et al. (2010) to last between 2720 and 2670 Ma. On the other hand, it supports Swager (1997) who determined a maximum age of 2684 Ma for a thrust which placed a 2705 ± 4 Ma komatiite tholeiite assemblage on top of a 2672 ± 12 Ma dacite (ages from Nelson, 1997). It also supports the interpretations of Weinberg et al. (2003b) who suggested that a contractional D_1 took place between 2685 and 2672 Ma, following an extensional event, D_{1e}, and accompanied by a change from volcanic-dominated to plutonic-dominated magmatism.

The two dike samples dated were deformed by D_2 and therefore the youngest of the two samples, dated at 2676 ± 9 Ma, can be conservatively used as an upper bound for this deformation event. It is possible, but unconfirmed, that D_2 was already active during dike intrusion so that S_2 foliation anisotropy controlled dike orientation. Czarnota et al. (2010) suggested that D_2 was diachronous throughout the Eastern Goldfields Superterrane having possibly started at around 2675 Ma in the Kurnalpi terrane, earlier

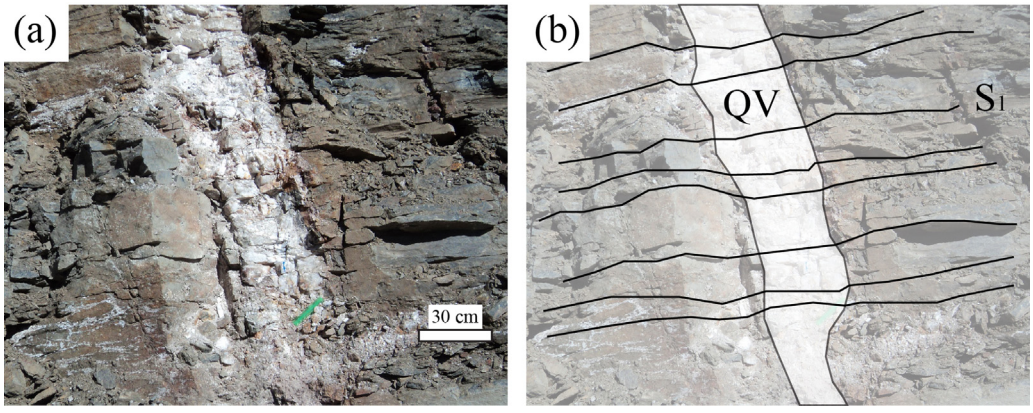

Fig. 15. (a) S_1 foliation in dolerite continues through mineralized quartz veins marked by jointing interpreted to be foliation-parallel fractures that post-date D_1. Wombola Dam Pit. (b) Same as (a) with interpretation lines. Photograph facing SW.

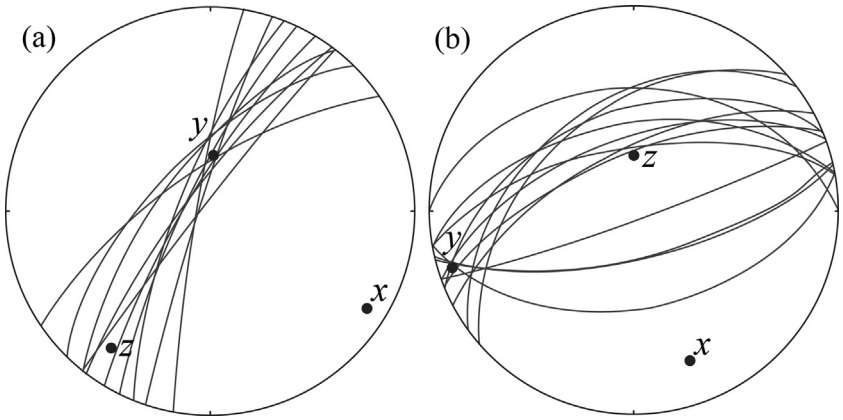

Fig. 16. Stereonet plot of quartz veins from the Wombola domain. (a) Veins from Wombola Dam Pit and two nearby trenches trending NE-SW intersecting along a line, *y*, plunging steeply to the north. (b) Veins from Wombola Pit and surrounding outcrops trending ENE-WSW and intersecting along a line, *y*, plunging gently to the WSW, ~90° from the *y*-axis in (a). Vein intersections are interpreted to represent intermediate *y* strain axis, and *x* and *z* are the maximum extension and shortening strain axis, respectively. Notice veins are approximately perpendicular to axial plane of upright large-scale fold in the pit, and *x*-axis is sub-parallel to the fold axis (stereonet in Fig. 14). Equal-area southern hemisphere projections.

than in the Kalgoorlie terrane and in broad agreement with our findings.

As mentioned earlier, the position of the Daisy Milano mining camp on the SW part of the nose of the large Bulong Dome is similar to the position of the Kanowna Belle gold deposit on the southern part of the Scotia-Kanowna Dome (Davis et al., 2010). Despite similarities between local D_1 and D_2 at Kanowna Belle and Daisy Milano, deformation at Kanowna Belle is much later than at Daisy Milano, and post-dates the felsic intrusion dated at 2656 ± 10 Ma (Davis et al., 2010; Squire et al., 2010). This lead Davis et al. (2010) to argue that local D_1 and D_2 at Kanowna Belle were related to a relatively late period of regional deformation, the D_{4b} of

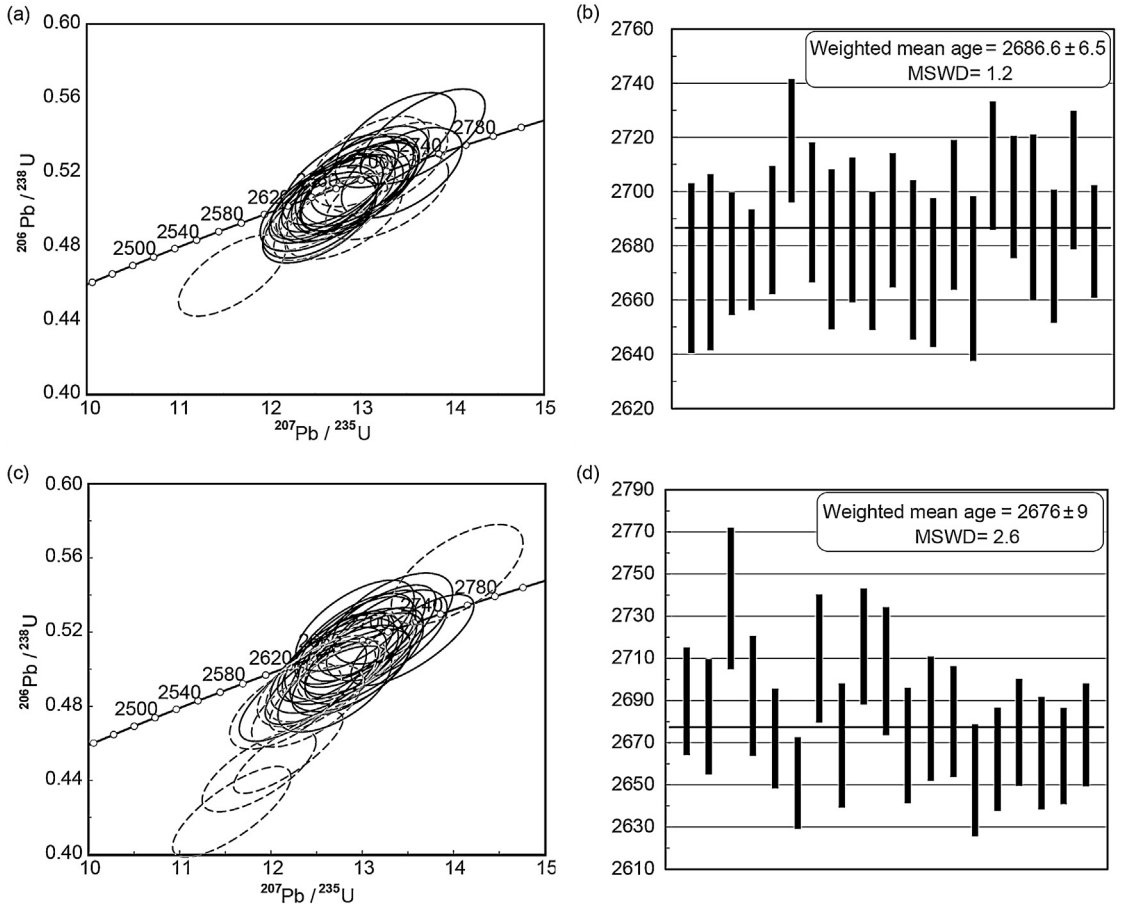

Fig. 17. LA-ICP-MS geochronological data for zircons analyzed from the two samples of tonalitic intrusion at Daisy Milano. (a) Concordia plot for all data for sample LC-75 from the 19-50 level at Daisy Milano mine. (b) Age-bar plot of the 21 concordant analyses from sample LC-75 and the weighted mean age. (c) Concordia plot for all data for sample LC-77 from the 35-52 level at Daisy Milano mine. (d) Age-bar plot of the 19 concordant geochronological data from sample LC-77 and the weighted mean age. For the concordia plots (a and c), discordant analyses are dashed lines. Also, the error ellipses for each data point are 2σ with propagated uncertainty. For the age-bar plots (b and d) the box heights are propagated 2σ values.

Blewett et al. (2010). In contrast, we argue that D_1 at Daisy Milano corresponds to the earliest regional event.

6.3. Timing and controls on gold mineralization

Gold mineralization differs between the two structural domains of the Daisy Milano mining camp. In the Daisy Milano domain, gold is found in narrow quartz veins at the contacts of porphyry dikes. The exact timing of emplacement of the felsic intrusions is unknown, but post-dates D_1 and was overprinted by S_2, and followed by gold mineralization. Gold mineralization at dike contacts and sub-parallel shear zones could be either related to D_2 or to later contact reactivation and shear zones development (Fig. 3). Gold is closely related to the N-S to NNW-SSE trending steep shear zones shown in Fig. 3, but these shear zones have not been documented here due to lack of exposure. Their orientation and our findings of late brittle faulting with slickenlines suggest reactivation as dextral-reverse (oblique) faults at a later deformation event.

A number of gold deposits in the Daisy Milano domain have steep NNW-trends and are immediately underneath moderately SW-dipping ultramafic layers (e.g.; Christmas Flats, Mirror, and Lorna Doone Pits and Daisy Milano underground). The attitude of the volcano-sedimentary sequence is a direct result of D_1, and the ultramafic layer may have provided an impermeable cap to the mineralizing fluids due to a combination of its natural low permeability perpendicular to foliation, and inability to fracture. Thus, the geometry set-up during D_1 may have controlled later mineralization by controlling the distribution of high permeability shear zones and impermeable ultramafic caps.

In the Wombola domain, gold is hosted by two sets of quartz veins, divided in accordance to their orientations and intersections (Fig. 16). The fact that veins developed preferentially in the hinge zone of the fold on the competent dolerite unit, combined with the strain axes derived from quartz vein attitudes (Figs. 15 and 16), suggest that mineralization took place during a shortening event with a broadly NE-SW z–y plane of the strain ellipsoid (Fig. 16). This could have been the same D_2 that folded the sill or could have been a later deformation event during which stress orientations were guided by the hinge zone.

7. Conclusions

The broad architecture and the main tectonic foliation in the Daisy Milano mining camp resulted from D_1, interpreted to have caused thrusting with top-to-the-NNW or -NW, with periods of stress relaxation recorded by normal movement towards the SSE or SE along the same plane. An alternative interpretation is that the region underwent pure shear shortening during D_1, perpendicular to S_1, where both reverse and normal movements developed simultaneously. D_2 overprinted early structures and gave rise to open folds and crenulation with a steep axial planar foliation trending NNW-SSE. The sequence was intruded by sills or dikes of plagioclase porphyritic tonalites. Sills were emplaced either before or during S_1, whereas the $\sim 2681 \pm 5$ Ma dikes intruded after D_1, possibly in the early stage of D_2 and are parallel to and foliated by S_2. We can thus bracket the duration of D_1 to between 2698 ± 3 Ma and 2681 ± 5 Ma corresponding to the ages of the Minerie Sequence and the dikes, respectively. We suggest further that D_2 could have started as early as 2681 ± 5 Ma when these dikes intruded. Given that in the Daisy Milano domain, mineralization is at the strained margins of these dikes, this age also provides an upper bound for the timing of gold deposition. Mineralization along later dextral-reverse N-S or NNW-SSE trending could post-date D_2. In contrast, in the Wombola domain, the presence of the 150 m thick competent dolerite gave rise to a broad upright F_2 fold with quartz veins formed along fractures at the hinge zone and at high angles to the axial plane of the fold. We conclude that the earliest deformation in the Kurnalpi terrane was likely a top-to-NW thrusting event with a strong pure shear component such as inferred by the early works in the Kalgoorlie Terrane, and that gold mineralization was contemporaneous to or post-dated D_2 controlled by the geometry set-up during thrusting.

Acknowledgements

This research was supported by ARC Linkage Grant LP110200747. We acknowledge the support of Silver Lake Resources and are particularly grateful for the support and discussions provided by Chris Banasik, Damien Keys, Jonathan Smalley, Antony Shephed and numerous other exploration and mine geologists at Daisy Milano. We also thank Ivan Zibra and Patrice Rey for helpful reviews.

Appendix A. Supplementary data

Supplementary data associated with this article can be found, in the online version, at http://dx.doi.org/10.1016/j.precamres.2015.05.013

References

Allen, C.M., Campbell, I.H., 2012. Identification and elimination of a matrix-induced systematic error in LA-ICP-MS $^{206}Pb/^{238}U$ dating of zircon. Chem. Geol. 332–333, 157–165.

Archibald, N.J., Bettenay, L.F., Binns, R.A., Groves, D.I., Gunthorpe, R.J., 1978. The evolution of Archaean greenstone terrains, Eastern Goldfields Province, Western Australia. Precambrian Res. 6, 103–131.

Barley, M.E., Krapez, B., Kositcin, N., Cassidy, K., Champion, D., Doyle, M., Brown, S., 2008. Terrane Stratigraphy of the Eastern Goldfields Superterrane, and Review of the Geotectonic History. Australian Mineral Industry Research Institute AMIRA P763, pp. 322.

Barley, M.E., Stuart, S.J.A., Krapez, B., Cas, R.A.F., 2002. Tectonostratigraphic Analysis of the Eastern Yilgarn Craton: An Improved Geological Framework for Exploration in Archean Terranes, AMIRA P437A. Australian Mineral Industry Research Institute Project P437A Final Report, pp. 263.

Bateman, R.J., Hagemann, S.G., McCuaig, T.C., Swager, C.P., 2001. Protracted gold mineralization throughout Archaean orogenesis in the Kalgoorlie camp, Yilgarn Craton, Western Australia: structural, mineralogical, and geochemical evolution. In: Hagemann, S.G., Neumayr, P., Witt, W.K. (Eds.), World-Class Gold Camps and Deposits in the Eastern Yilgarn Craton, Western Australia, with Special Emphasis on the Eastern Goldfields Province. Western Australia Geological Survey, pp. 63–98.

Blewett, R.S., Czarnota, K., Henson, P.A., 2010. Structural-event framework for the eastern Yilgarn Craton, Western Australia, and its implications for orogenic gold. Precambrian Res. 183, 203–229.

Blewett, R.S., Czarnota, K., 2007. Tectonostratigraphic Architecture and Uplift History of the Eastern Yilgarn Craton. Module 3: Terrane Structure, Project Y1-P763. Geoscience Australia.

Bucci, L.A., McNaughton, N.J., Fletcher, I.R., Groves, D.I., Kositcin, N., Stein, H.J., Hagemann, S., 2004. Timing and duration of high-temperature gold mineralization and spatially associated granitoid magmatism at Chalice, Yilgarn Craton, Western Australia. Econ. Geol. 99, 1123–1144.

Cassidy, K.F., Champion, D.C., Krapež, B., Barley, M.E., Brown, S.J.A., Blewett, R.S., Groenewald, P.B., Tyler, I.M., 2006. A Revised Geological Framework for the Yilgarn Craton, Western Australia, Record 2006/8, 8. Western Australia Geological Survey.

Czarnota, K., Champion, D.C., Goscombe, B., Blewett, R.S., Cassidy, K.F., Henson, P.A., Groenewald, P.B., 2010. Geodynamics of the eastern Yilgarn Craton. Precambrian Res. 183, 175–202.

Davis, B.K., Blewett, R.S., Squire, R., Champion, D.C., Henson, P.A., 2010. Granite-cored domes and gold mineralisation: architectural and geodynamic controls around the Archaean Scotia-Kanowna Dome, Kalgoorlie Terrane, Western Australia. Precambrian Res. 183, 316–337.

Davis, B.K., Hickey, K.A., Rose, S., 2001. Superposition of gold mineralization on pre-existing carbonate alteration: structural evidence from the Mulgarrie Gold Deposit Yilgarn Craton. Aust. J. Earth Sci. 48, 131–149.

Davis, B.K., Maidens, E., 2003. Archaean orogen-parallel extension: evidence from the northern Eastern Goldfields Province, Yilgarn Craton. Precambrian Res. 127, 229–248.

Dunphy, J.M., Fletcher, I.R., Cassidy, K.F., Champion, D.C., 2003. Compilation of SHRIMP U–Pb geochronological data, Yilgarn Craton, Western Australia, 2001–2002, Record 2003/15. Geoscience Australia, pp. 139.

Griffin, T.J., Hickman, A.H., 1988. Lake Lefroy, WA, Sheet 3235, 1st ed. Geological Survey Western Australia, Perth.
Groves, D.I., Batt, W.D., 1984. Spatial and temporal variations in Archaean metallogenic associations in terms of evolution of granitoid-greenstone terrains with particular emphasis on the Western Australian Shield. In: Kröner, A., Hanson, G.N., Goodwin, A.M. (Eds.), Archaean Geochemistry: The Origin and Evolution of the Archaean Continental Crust. Springer-Verlag, Berlin, pp. 73–98.
Groves, D.I., Goldfarb, R.J., Knox-Robinson, C.M., Ojala, J., Gardoll, S., Yun, G.Y., Holyland, P., 2000. Late-kinematic timing of orogenic gold deposits and significance for computer-based exploration techniques with emphasis on the Yilgarn Block, Western Australia. Ore Geol. Rev. 17, 1–38.
GSWA, 2008. 1:500,000 Interpreted Bedrock Geology of Western Australia, 1:500,000 Tectonic Subdivisions of Western Australia, 2010 Update ed. Geological Survey of Western Australia, Perth.
Hammond, R.L., Nisbet, B.W., 1992. Towards a structural and tectonic framework for the central Norseman-Wiluna greenstone belt, Western Australia. In: Glover, J.E., Ho, S.E. (Eds.), The Archaean: Terrains, Processes and Metallogeny. Geology Department (Key Centre) & University Extension, vol. 22. University of Western Australia, Perth, pp. 39–50.
Hickman, A.H., 1986. Stratigraphy, Structure and Economic Geology of the Mount Monger Area, Eastern Goldfields Province, Report No. 16. Geological Survey of Western Australia, Perth.
Hodkiewicz, P.F., Weinberg, R.F., Gardoll, S.J., Groves, D.I., 2005. Complexity gradients in the Yilgarn Craton: fundamental controls on crustal-scale fluid flow and the formation of world-class orogenic-gold deposits. Aust. J. Earth Sci. 52, 831–841.
Holcombe, R., 2014. Orientated Drillcore: Measurement, Conversion, and QA/QC Procedures for Structural and Exploration Geologists. Holcombe Coughlin Oliverand Associates, pp. 1–36.
Jones, S., 2007. North Monger Area, Structural Mapping. RSG Global Consulting Party Limited, West Perth, pp. 17.
Knight, J.T., Groves, D.I., Ridley, J.R., 1993. The Coolgardie Goldfield, Western Australia: district-scale controls on and Archaean gold camp in an amphibolite facies terrane. Mineral. Depos. 28, 436–456.
Ludwig, K.R., 2003. Isoplot/Ex Version 3.00 A Geochronological Toolkit for Microsoft Excel. Berkeley Geochronological Centre Special Publication No. 4.
Martyn, J.E., 1987. Evidence for structural repetition in the greenstones of the Kalgoorlie District, Western Australia. Precambrian Res. 37, 1–18.
McGoldrick, K.L., Squire, R.J., Cas, R.A.F., Briggs, M., Tunjic, J., Allen, C.M., Campbell, I.H., Hayman, P.C., 2013. The largest Au deposits in the St Ives Goldfield (Yilgarn Craton, Western Australia) may be located in a major Neoarchean volcano-sedimentary depo-centre. Mineral. Depos. 48, 861–881.
Miller, J., Blewett, R., Tunjic, J., Connors, K., 2010. The role of early formed structures on the development of the world class St Ives Goldfield, Yilgarn, WA. Precambrian Res. 183, 292–315.
Morey, A.A., Weinberg, R.F., Bierlein, F.P., 2007. The structural controls of gold mineralisation within the Bardoc Tectonic Zone, Eastern Goldfields Province, Western Australia: implications for gold endowment in shear systems. Mineral. Depos. 42, 583–600.
Nelson, D.R., 1997. Evolution of the Archaean granite-greenstone terranes of the Eastern Goldfields, Western Australia: SHRIMP U–Pb zircon constraints. Precambrian Res. 83, 57–81.
Passchier, C.W., 1994. Structural geology across a proposed Archaean terrane boundary in the eastern Yilgarn craton, Western Australia. Precambrian Res. 68, 43–64.
Paton, C., Woodhead, J.D., Hellstrom, J.C., Hergt, J.M., Greig, A., Maas, R., 2010. Improved laser ablation U–Pb zircon geochronology through robust downhole fractionation correction. Geochem. Geophys. Geosyst. 11.
Platt, J.P., Allchurch, P.D., Rutland, R.W.R., 1978. Archaean tectonics in the Agnew supracrustal belt, Western Australia. Precambrian Res. 7, 3–30.
Squire, R.J., Allen, C.M., Cas, R.A.F., Campbell, I.H., Blewett, R.S., Nemchin, A.A., 2010. Two cycles of voluminous pyroclastic volcanism and sedimentation related to episodic granite emplacement during the late Archean: Eastern Yilgarn Craton, Western Australia. Precambrian Res. 183, 251–274.
Swager, C., Griffin, T.J., 1990. An early thrust duplex in the Kalgoorlie-Kambalda greenstone belt, Eastern Goldfields Province, Western Australia. Precambrian Res. 48, 63–73.
Swager, C.P., 1997. Tectono-stratigraphy of late Archaean greenstone terranes in the southern Eastern Goldfields, Western Australia. Precambrian Res. 83, 11–42.
Trofimovs, J., Davis, B.K., Cas, R.A.F., 2004. Contemporaneous ultramafic and felsic intrusive and extrusive magmatism in the Archaean Boorara Domain, Eastern Goldfields Superterrane, Western Australia, and its implications. Precambrian Res. 131, 283–304.
VL, 2007. Mt Monger Project, Interpreted Geology LM4950. Perilya Limited.
Weinberg, R.F., Hodkiewicz, P.F., Groves, D.I., 2004. What controls gold distribution in Archean terranes? Geology 32, 545–548.
Weinberg, R.F., van der Borgh, P., 2008. Extension and gold mineralization in the Archean Kalgoorlie Terrane, Yilgarn Craton. Precambrian Res. 161, 77–88.
Weinberg, R.F., Van der Borgh, P., Hodkiewicz, P., Groves, D.I., 2003a. AMIRA Project P511, Melbourne.
Weinberg, R.F., van der Borgh, P., Moresi, L., 2003b. Timing of deformation in the Norseman-Wiluna Belt, Yilgarn Craton, Western Australia. Precambrian Res. 120, 219–239.
Weinberg, R.F., van der Borgh, R., Bateman, R.J., Groves, D.I., 2005. Kinematic history of the Boulder-Lefroy shear zone system and controls on associated gold mineralization, Yilgarn craton, Western Australia. Econ. Geol. 100, 1407–1426.
Westchester, 1993. Geology of the Mirror Pit. Westchester Mining, Mt Monger, WA.
Williams, P.R., Currie, K.L., 1993. Character and regional implication of the sheared Archaean granite-greenstone contact near Leonora, Western Australia. Precambrian Res. 62, 343–365.
Williams, P.R., Nisbet, B.W., Etheridge, M.A., 1989. Shear zones, gold mineralization and structural history in the Leonora District, Eastern Goldfields Province, Western Australia. Aust. J. Earth Sci. 36, 383–403.
Williams, P.R., Whitaker, A.J., 1993. Gneiss domes and extensional deformation in the highly mineralized Archean-Eastern-Goldfields Province, Western-Australia. Ore Geol. Rev. 8, 141–162.
Witt, W.K., 2001. Tower Hill gold deposit, Western Australia: an atypical, multiply deformed Archaean gold-quartz vein deposit. Aust. J. Earth Sci. 48, 81–99.
Witt, W.K., Swager, C.P., 1989. Structural setting and geochemistry of Archaean I-type granites in the Bardoc-Coolgardie area of the Norseman-Wiluna Belt, Western Australia. Precambrian Res. 44, 323–351.